THE JOURNAL OF PHYSICAL CHEMISTRY C

Article

pubs.acs.org/JPCC

Size- and Composition-Dependent Energy Transfer from Charge Transporting Materials to ZnCuInS Quantum Dots

Xi Yuan,[†,‡] Jialong Zhao,*[,†] Pengtao Jing,[†,§] Wenjin Zhang,[∥] Haibo Li,[⊥] Ligong Zhang,[†] Xinhua Zhong,[∥] and Yasuaki Masumoto*[,§]

[†]State Key Laboratory of Luminescence and Applications, Changchun Institute of Optics, Fine Mechanics and Physics, Chinese Academy of Sciences, 3888 Eastern South Lake Road, Changchun 130033, China

[‡]Graduate School of Chinese Academy of Sciences, Beijing 100039, China

[§]Institute of Physics, University of Tsukuba, Tsukuba, Ibaraki 305-8571, Japan

[∥]State Key Laboratory of Chemical Engineering, Department of Chemistry, East China University of Science and Technology, Shanghai 200237, China

[⊥]Key Laboratory of Functional Materials Physics and Chemistry of the Ministry of Education, Jilin Normal University, Siping 136000, China

Supporting Information

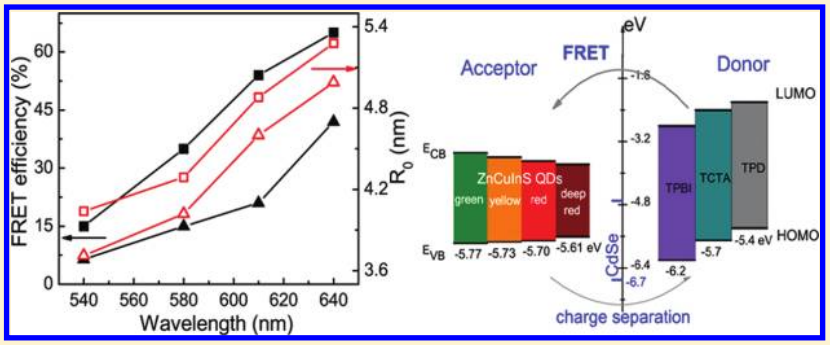

ABSTRACT: We studied the energy transfer processes from organic charge transporting materials (CTMs) to ZnCuInS (ZCIS) quantum dots (QDs) with different emission wavelength by steady-state and time-resolved photoluminescence (PL) spectroscopy. The change in the PL excitation intensity of the ZCIS QDs and the PL decay time of the CTMs clearly demonstrated an efficient energy transfer process in the ZCIS/CTM blend films. It was found that the efficiency of Förster resonance energy transfer significantly increases with increasing the particle size and decreasing the Zn content in the QDs, which is well consistent with the estimated Förster radii (R_0) varying from 3 to 5 nm. In addition, the PL quenching of the QDs related to the charge separation process was also observed in some of the samples. The energy transfer and charge separation processes in the films were well explained based on the band alignment between the ZCIS QDs and CTMs.

INTRODUCTION

Hybrid organic/quantum dot (QD) optoelectronic devices such as light-emitting diodes (LEDs)[1−8] and photovoltaic cells[9−12] are of significant technological interests as they combine the tunable band gaps and durability of colloidal semiconductor QDs with the flexibility and low processing cost of organic materials. However, most of the exploration of QD applications containing heavy-metal constituents such as Cd and Pb could potentially hinder the ultimate research transformation and commercialization of QD optoelectronic devices. As a new kind of nanomaterials, I−III−VI based semiconductors such as $CuInS_2$ have markedly low toxicity, a large absorption coefficient (10^5 cm^{-1}) and size-tunable emissions, considered to be suitable for applications as light-emitting and solar-harvesting materials.[13−19] The photoluminescence (PL) wavelength of the $CuInS_2$ QDs could be tuned from 950 to 500 nm by decreasing the particle size to 2 nm;[15,16] however, the small-sized nanoparticles are unstable and possess low emission efficiency.[20,21] The heavy metal-free ZnCuInS or $CuInS_2$−ZnS alloyed (ZCIS) QDs have exhibited highly efficient and widely tunable PL from the visible to NIR region by varying not only the size but also the composition of particles.[20−23] These properties make ZCIS QDs relevant to applications in solid state lighting and full color displays.

Recently, Tan et al. have prepared green, yellow, or red emission QD/organic LEDs with the maximum luminance of 1600 cd/m^2, using ZCIS QDs as emitting materials.[24] More recently, the maximum luminance for yellow emission ZCIS

Received: April 18, 2012
Revised: May 11, 2012
Published: May 14, 2012

 © 2012 American Chemical Society dx.doi.org/10.1021/jp3037236 | J. Phys. Chem. C 2012, 116, 11973−11979

QD-LEDs fabricated by Zou et al. have reached 2100 cd/m^2.[25] These results mean that the heavy metal-free ZCIS QD-LEDs are still at the early stage of development and the improvement in their performance is greatly required. It is known that the highly efficient archetypical QD-LEDs are fabricated by sandwiching an inorganic QD layer between two layers of organic charge transporting materials (CTMs), in which excitons in the QD layer in the QD-LEDs can be generated by exciton energy transfer and charge injection from the organic molecules.[1,2,4,5] The performance of QD-LEDs should be enhanced by maximizing Förster resonance energy transfer (FRET) from the CTMs to QDs. The FRET describes a nonradiative transfer process of excitation energy from a donor fluorophore to an acceptor through a dipole−dipole interaction.[26−28] Therefore, according to the Förster theory, the energy transfer efficiency is dependent not only on the donor−acceptor separation distance but also on the spectral overlap integral between the emission spectrum of the donor and the absorption spectrum of the acceptor, which is usually expressed by the Förster radius.[26] Clapp et al. demonstrated a clear dependence of the energy transfer efficiency on the spectral overlap between CdSe QD donor and Cy3 dye acceptor by tuning the size of QDs.[29] Sadhu et al. showed the variation of the energy transfer efficiency from 14% to 47% with changing the Cd/Zn ratio in $Cd_xZn_{1-x}S$ alloy nanocrystals due to the change of the spectral overlap.[30] Lunz et al. reported the stronger concentration-dependent energy transfer processes in QD monolayers with a broader emission band because of the self-overlap of QDs.[31] However, the type II energy alignment usually results in the coexistence of energy transfer and charge separation processes in the hybrid organic/inorganic nanocomposites.[32] The energy transfer and charge separation efficiency could be controlled by using the shell structure and material to change the distance between CdSe QDs and hole transporting materials in our previous reports.[33,34] For the improvement in the performance of the environment-friendly ZCIS QD-LEDs, it is necessary to understand the issues about the energy transfer processes and the energy level alignment between ZCIS QDs and CTMs. However, to date, no report about them has been given yet.

In this work, we report the study on the energy transfer processes between ZCIS/ZnS core/shell QDs showing green (G), yellow (Y), red (R), and deep red (DR) emissions and the frequently used CTMs such as 1,3,5-tris(*N*-phenylbenzimidazol-2,yl)benzene (TPBI), 4,4′,4″-tris(carbazol-9-yl)-triphenylamine (TCTA), and *N*,*N*′-di(3-methylphenyl)-*N*,*N*′-di(phenyl)benzidine (TPD). The PL intensities and lifetimes of the ZCIS QDs and CTMs in the films were measured by steady-state and time-resolved PL spectroscopy to demonstrate the energy transfer process. Then, the effects of the size and the composition of the ZCIS QDs on the Förster radius and FRET efficiency were studied and discussed. Finally, the PL quenching of the QDs in some of the QD/CTM (TCTA and TPD) blend films was explained in terms of the charge separation process based on the conduction and valence levels for ZCIS QDs estimated by cyclic voltammetry and optical spectroscopy.

EXPERIMENTAL SECTION

Preparation and Characterization of ZnCuInS QDs. The ZCIS core QDs and ZCIS/ZnS core/shell QDs used in this experiment were synthesized by the same method as we used in our previous work.[21] The details of the QD synthesis are described in the Supporting Information. The size and shape of the QDs were measured by a Tecnai G2 transmission electron microscope (TEM) operated at 200 kV. Samples for TEM were prepared by drop-casting QDs dispersed in toluene onto carbon-coated 200-mesh copper grids. X-ray diffraction (XRD) patterns of the QDs were collected by a Rigaku XRD spectrometer with a Cu Kα line of 0.15418 nm at a scanning step of 0.02°. The energy dispersive X-ray spectroscopy (EDS) for the elemental analysis of the inorganic QDs was measured by using a Philips ESEM XL30 scanning electron microscope. Thermogravimetric analysis (TGA) was performed to examine the quantity of organic materials on the QD surface on a PerkinElmer Pyris Diamond TG/DTA Instruments under N_2 atmosphere at a heating rate of 10 °C/min within a temperature range of 40−800 °C. Energy levels of the QDs were obtained from cyclic voltammetry measurements and absorption spectra.[16,32] The cyclic voltammetry measurements were performed on an EG&G 283 (Princeton Applied Research) potentiostat/galvanostat system, and the details are described in the Supporting Information.

Preparation of ZnCuInS QD/Charge Transporting Materials Blend Films. The QD/CTM blend films were prepared by spin coating the appropriate mixtures of the QDs (20−60 μM) and CTMs (10 mg/mL) in chloroform onto quartz substrates at a speed of 1200 rpm. The QD/CTM molar ratio was changed from 1/15 to 1/60. The QD/PMMA (poly(methyl methacrylate), molecular weight of 15 000, transparent in the visible spectral region) blend films were prepared as reference samples. The molar concentration of the ZCIS QDs was determined by combining XRD, TEM, EDS, and TGA,[35,36] and the details are described in the Supporting Information. The thicknesses of blend films were measured as 30−50 nm by a KLA-Tencor P-16$^+$ surface profiler.

Optical Characterization. The absorption spectra were recorded by a UV-3101PC UV−vis/NIR scanning spectrophotometer (Shimadzu). The PL and excitation spectra were recorded by an F-4500 spectrophotometer (Hitachi) equipped with a 150 W Xe arc lamp. The time-resolved PL spectra were measured by an FL920 fluorescence lifetime spectrometer (Edinburgh Instruments). The excitation source was a hydrogen flash lamp (nF900) with a pulse width of 1.5 ns. Fluorescence quantum yields of the ZCIS QDs were estimated by comparison of the fluorescence intensity with standard dye solutions with the same optical density at the excitation wavelength and similar fluorescence wavelength. All measurements were carried out at room temperature. The PL decay kinetics was deconvolution fitted by using the ASUFIT program.

RESULTS AND DISCUSSION

Figure 1 shows UV−visible absorption and normalized PL spectra of ZCIS/ZnS core/shell QDs. The G-, Y-, R-, and DR-ZCIS/ZnS QDs showing emissions at 540, 580, 610, and 640 nm, respectively, and high PL quantum yields of over 40% were synthesized by incorporating Zn into $CuInS_2$ QDs and then coating a ZnS shell layer. As seen in Figure 1, the absorption onset of the obtained QDs is blueshifted to green from the deep red wavelength side with decreasing the particle size from 4.6 to 2.8 nm and increasing Zn content (Zn/Cu molar ratio in core) from 0.2/1 to 0.6/1, which could be explained by quantum confinement and the alloy structure of ZnS (bandgap of 3.7 eV) and $CuInS_2$ (bandgap of 1.53 eV).[21,23] The size and composition of the QDs were estimated by TEM and EDS as shown in Figures S1 and S2 of the Supporting Information,

dx.doi.org/10.1021/jp3037236 | J. Phys. Chem. C 2012, 116, 11973−11979

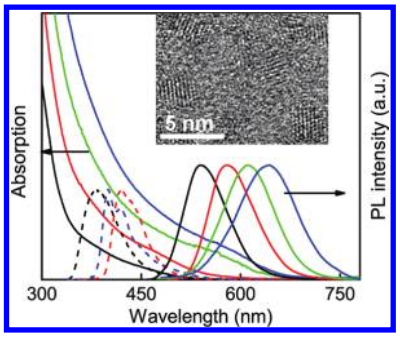

Figure 1. UV−visible absorption and PL spectra (solid lines) of ZCIS/ZnS core/shell QDs with emission peak position at 540 nm (black lines), 580 nm (red lines), 610 nm (green lines), and 640 nm (blue lines) and PL spectra of TPBI (black dashed line), TCTA (red dashed line), and TPD (blue dashed line) under excitation at 320 nm. A high-resolution TEM image of G-ZCIS/ZnS core/shell QDs is shown in the inset.

respectively. The high-resolution TEM image of G-ZCIS/ZnS core/shell QDs exhibits clear lattice fringes as shown in the inset of Figure 1, which suggests the highly crystalline nature. XRD patterns for the ZCIS/ZnS core/shell QDs shown in Figure S3 of the Supporting Information present the characteristic peaks of the zinc blende (cubic) structure. The diffraction peaks of the ZCIS/ZnS QDs slightly shift to larger angles as increasing Zn content, which is consistent with the smaller Zn^{2+} cationic radius than those of Cu^{+} and In^{3+}, corresponding to the lattice constants of 5.468, 5.453, 5.437, and 5.420 Å for DR-, R-, Y-, G-QDs, respectively. However, the normalized PL spectra of organic CTMs (TPBI, TCTA, and TPD) are also shown in Figure 1. It is clearly observed that there is a spectral overlap between the absorption of ZCIS/ZnS QDs (acceptor) and the PL emission of the CTMs (donor) as a prerequisite for FRET.[26,32] The distinctly tunable absorption spectra of ZCIS/ZnS QDs means that the size and composition should influence the FRET process between the QDs and CTMs.

The PL excitation spectra of the R-ZCIS/ZnS core/shell QDs in QD/PMMA (TPBI and TCTA) blend films with different molar ratio of the QD/CTM are shown in Figure 2a,b. The PL excitation spectra are normalized at a wavelength of 425 nm without the absorption from TPBI (TCTA) as shown in Figure S4 of the Supporting Information. The relative enhancement in the PL excitation intensity of the QDs in the blend films is clearly observed at the absorption wavelength of the CTMs, compared with that in PMMA film, indicating an energy transfer process from the CTMs to QDs.[32] The similar PL excitation intensity enhancement was also observed in QD/TPD blend films as shown in Figure S5 of the Supporting Information, providing a potent evidence that energy transfer also takes place between TPD and ZCIS/ZnS QDs.[32,34]

To clarify the energy transfer dynamics, the PL decays of CTMs were measured in the organic/inorganic hybrid systems. Figure 2c,d shows the evolution of the time-resolved PL spectra of TPBI and TCTA in R-ZCIS/ZnS QD/CTM blend films with different QD/molecule molar ratios under the excitation wavelength of 320 nm. The PL decays of TPBI (TCTA) molecules became faster in the blend films because the energy transfer process is an additional nonradiative de-excitation path for donors, which expresses as $1/\tau_{donor-acceptor} = 1/\tau_{donor} + k_{ET}$, where $\tau_{donor-acceptor}$ and τ_{donor} are the PL lifetimes of TPBI (TCTA) donor in blend and neat films,[26] and k_{ET} is the energy transfer rate. We analyzed the PL decays of the TPBI (TCTA) molecules by a biexponential function with two time components (τ_i) and weights (A_i). The average lifetimes were obtained by the relationship $\tau_{av} = (A_1\tau_1^2 + A_2\tau_2^2)/(A_1\tau_1 +$

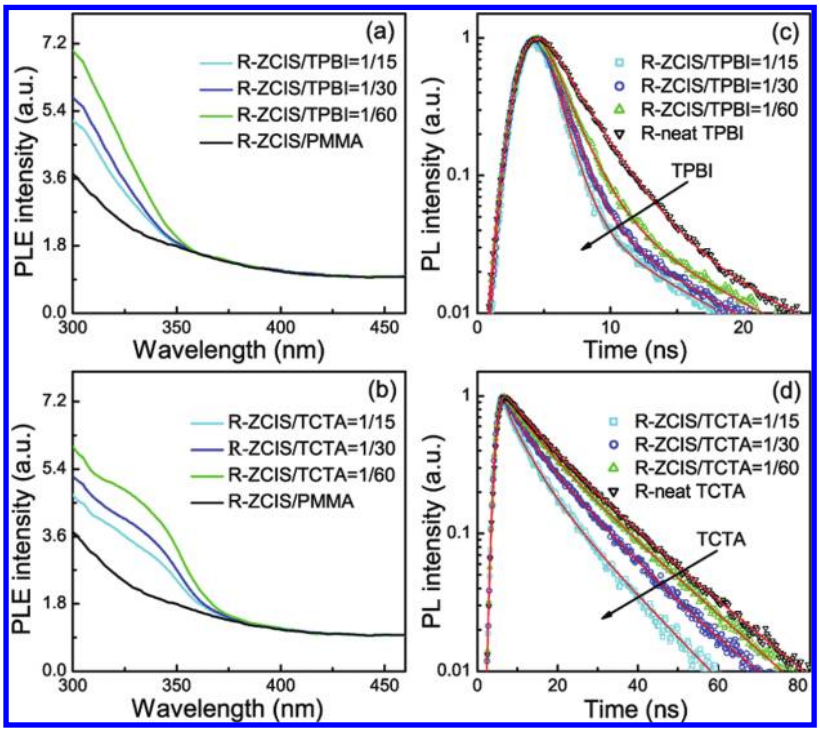

Figure 2. Normalized PL excitation spectra (a,b) of R-ZCIS/ZnS QDs and temporal change of PL intensities of CTMs (c,d) in QD/TPBI (a,c) and QD/TCTA (b,d) blend films with different QD/CTM molar ratio (1/15, 1/30, and 1/60). The solid red lines in panels c and d represent deconvolution fitting curves.

dx.doi.org/10.1021/jp3037236 | J. Phys. Chem. C 2012, 116, 11973−11979

$A_2\tau_2$). From the deconvolution fitting of the decay curves, the average lifetimes of the CTMs with QD/CTM molar ratios of 1/15, 1/30, 1/60, and neat CTMs were summarized in Table 1.

Table 1. Average PL Lifetimes of CTMs for R-ZCIS QD/TPBI (TCTA) Molar Ratios of 1/15, 1/30, 1/60, and Neat CTMs, Corresponding Energy Transfer Efficiencies, and Rates in the Organic/Inorganic Hybrid System

	PL lifetime (ns)		efficiency (%)		rate (s^{-1})	
samples	TPBI	TCTA	TPBI	TCTA	TPBI	TCTA
1/15	1.0	9.2	62	41	6.2×10^8	4.5×10^7
1/30	1.2	12.4	54	21	4.5×10^8	1.7×10^7
1/60	1.6	14.1	38	9.6	2.4×10^8	0.7×10^7
neat TPBI (TCTA)	2.6	15.6				

The corresponding energy transfer efficiencies and rates were obtained by expressions $1 - \tau_{donor-acceptor}/\tau_{donor}$ and $1/\tau_{donor-acceptor} - 1/\tau_{donor}$, respectively,[26] also shown in Table 1. It was noted that the energy transfer efficiency decreases as increasing the concentration of the CTMs. On the basis of the Förster theory, the longer donor−acceptor distance makes the energy transfer less effective.[26] Most of TPBI (TCTA) molecules are far from the QD surface when the concentration of CTMs is high, resulting in a small change of PL lifetime as seen in Figure 2c,d. When the concentration of CTMs is low, most of the molecules distributed near the surface of QDs, leading to a markedly shortening of the donor PL lifetime. This result confirms that the FRET process in the blend films of TPBI (TCTA) and ZCIS/ZnS QDs is dependent on the donor/acceptor molar ratio due to the change of the average distance between TPBI (TCTA) donor molecules and the QD acceptors.

In order to understand the energy transfer dynamics in ZCIS QD/TPBI(TCTA) blend films with different QD emissions, the PL decay curves of TPBI and TCTA in the blend films were measured, as shown in Figure 3. The PL decay of the donor molecules is difficult to measure if the concentration of the CTM in the film is too low. Additionally, the PL decay curves of the donor molecules cannot reflect the information about the energy transfer dynamics when the concentration of the CTM in the film is too high. Therefore, we chose 1/30 as the suitable QD/CTM molar ratio for investigating the energy transfer process between ZCIS/ZnS QDs and TPBI (TCTA). It is found that the PL decay of the TPBI (TCTA) became slower with decreasing the emission wavelength of the ZCIS QDs. The average PL lifetimes of TPBI and TCTA in G-, Y-, R-, and DR-QD/TPBI (TCTA) blend films were obtained as 2.2, 1.7, 1.2, and 0.9 ns and 14.6, 13.2, 12.4, and 9.0 ns, respectively. The corresponding energy transfer efficiencies and rates were obtained to be 15%, 35%, 54%, and 65% and 0.7, 2.0, 4.5, and 7.3×10^8 s^{-1} for QD/TPBI blend films, and to be 6.4%, 15%, 21%, and 42% and 0.4, 1.2, 1.7, and 4.7×10^7 s^{-1} for QD/TCTA blend films, respectively. It is clearly shown that the energy transfer efficiency and rate increases with the redshift of the QD emission, indicating the spectrally dependent FRET process.

The efficiencies as a function of the QD emission wavelength are shown in Figure 4. For the analysis of the spectrally dependent FRET process in detail, we need to estimate the spectral overlap integral between acceptor absorption and

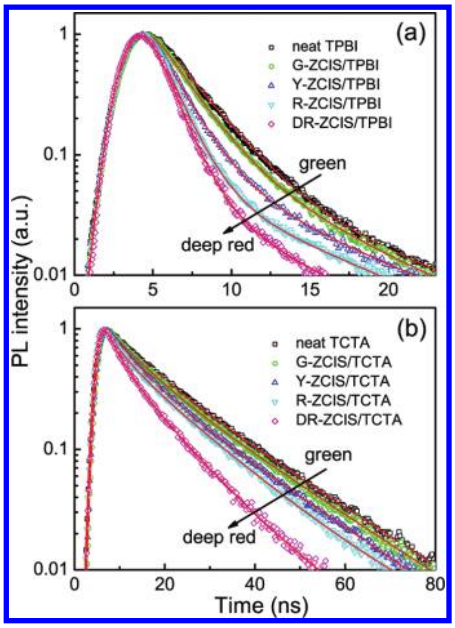

Figure 3. Temporal change of PL intensities of TPBI (a) and TCTA (b) in G-, Y-, R-, and DR-ZCIS/ZnS QD/CTM blend films with the same QD/TPBI (TCTA) molar ratio of 1/30. The solid red lines represent deconvolution fitting curves. The excitation wavelength is 320 nm.

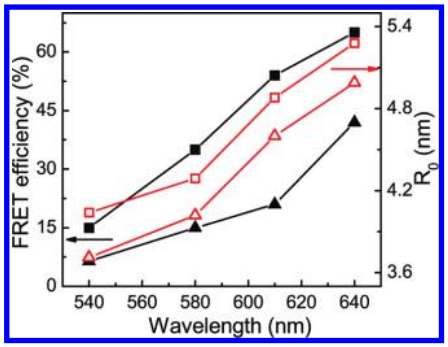

Figure 4. Efficiencies of energy transfer from TPBI (black solid squares) and TCTA (black solid triangles) to ZCIS/ZnS QDs as a function of the QD emission wavelength. The molar ratio of the QD/CTM in blend films is taken as 1/30. The calculated Förster radii (R_0) of G-, Y-, R-, and DR-ZCIS/ZnS QDs in the QD/TPBI (red empty squares) and TCTA (red empty triangles) hybrid systems are also shown in the figure.

donor emission and the Förster radius. The overlap integral J is defined as follows:[26]

$$J = \int_0^\infty F_D(\lambda)\varepsilon_A(\lambda)\lambda^4 d\lambda \quad (1)$$

where $F_D(\lambda)$ is the normalized donor emission spectrum, and $\varepsilon_A(\lambda)$ is the acceptor molar extinction coefficient. The Förster radius R_0, which is defined as the separation distance corresponding to 50% FRET efficiency, can be expressed as[26]

$$R_0 = \left(\frac{9000(\ln 10)Q_D\kappa^2}{128\pi^5 N_A n_D{}^4}J\right)^{1/6} \quad (2)$$

where Q_D is the quantum yield of the donor, N_A is Avogadro's number, n_D refers to the refractive index of the medium, and κ is a parameter that depends on the relative orientation of the

dx.doi.org/10.1021/jp3037236 | J. Phys. Chem. C 2012, 116, 11973−11979

donor and acceptor dipoles. We used $\kappa^2 = 2/3$ here for randomly oriented dipoles.

From eq 1, the overlap integral is dependent on the molar extinction coefficient ε_A of acceptor at the donor emission wavelength. Moreels et al. and Peng et al. have proved that the molar extinction coefficient increases with increasing the particle size.[35,36] However, the molar extinction coefficient at 400 nm around the emission wavelength of TPBI or TCTA should increase as decreasing the Zn content in the QDs because the band gap energy of ZnS (3.7 eV) is larger than that of CTMs. In our experiment, the molar extinction coefficient $\varepsilon_A(\lambda)$ of QDs with different emission peaks was estimated by Lambert–Beer's law $A = \varepsilon_A CL$, where A is the absorbance, C is the molar concentration (mol/L) of the QDs, and L is the path length (cm) of the radiation beam.[36] The molar extinction coefficients at 400 nm of G-, Y-, R-, and DR-ZCIS QDs are shown in Table 2. We observed that the DR-ZCIS QDs with

Table 2. Molar Extinction Coefficient (ε_A) at Wavelength of 400 nm for ZCIS QDs and Spectral Overlap Integrals J for TPBI (TCTA)/ZCIS QD Hybrid System

		J (M^{-1} cm^3)	
samples	ε_A (400 nm) (M^{-1} cm^{-1})	TPBI	TCTA
G-ZCIS	0.85×10^5	2.09×10^{-13}	1.77×10^{-13}
Y-ZCIS	1.18×10^5	3.01×10^{-13}	2.85×10^{-13}
R-ZCIS	2.48×10^5	6.47×10^{-13}	6.42×10^{-13}
DR-ZCIS	4.08×10^5	10.47×10^{-13}	10.42×10^{-13}

the largest particle size and the least Zn content exhibit the largest molar extinction coefficient. The overlap integral between ZCIS QDs and donor TPBI or TCTA was calculated from eq 1 as summarized in Table 2. It is clearly shown that the overlap integral rapidly increases with the change of PL color of QDs from green to deep red. Combining the overlap integral of different ZCIS QDs, the value of the Förster radius was calculated from eq 2, as plotted in Figure 4. In the previous reports, the Förster radius of CdSe QD/organic molecule system was estimated to about 3–8 nm,[30,37–40] which is quantitatively consistent with that of the donor–acceptor system of TPBI (TCTA) and ZCIS QDs. As seen in Figure 4, the Förster radius for TPBI (TCTA) system increases from 4.0 (3.7) nm to 5.3 (5.0) nm with the redshift of the absorption onset of ZCIS QDs, showing a similar trend in the energy transfer efficiency. The result is consistent with the Förster theory: the energy transfer efficiency for a donor–acceptor pair depends on Förster radius (R_0) as $\eta_{ET} = R_0^6/(R_0^6 + r^6)$. The redder emission QDs have a larger spectral overlap with TPBI (TCTA) than greener QDs, resulting in a larger Förster radius and more efficient energy transfer. The energy transfer efficiency from TPBI (TCTA) to DR-ZCIS QDs with large particle size and low Zn content in the QDs can achieve 65% (42%). This means that the energy transfer efficiency can be improved by controlling the size and composition of acceptor ZCIS QDs because of the change in the spectral overlap between CTMs and ZCIS QDs.

In contrast to the enhancement in the QD PL due to energy transfer process, the charge separation at the interface of QDs/organic molecules will quench the PL of QDs, which may influence the performance of the QD-LED.[5] Thus, it is important to confirm whether the charge separation process occurs in ZCIS QD/CTM blend films. The PL decay curves of ZCIS/ZnS QDs with different emission wavelength in the CTMs and PMMA under excitation wavelength of 425 nm are shown in Figure 5. It is clearly noted that PL lifetimes of G- and

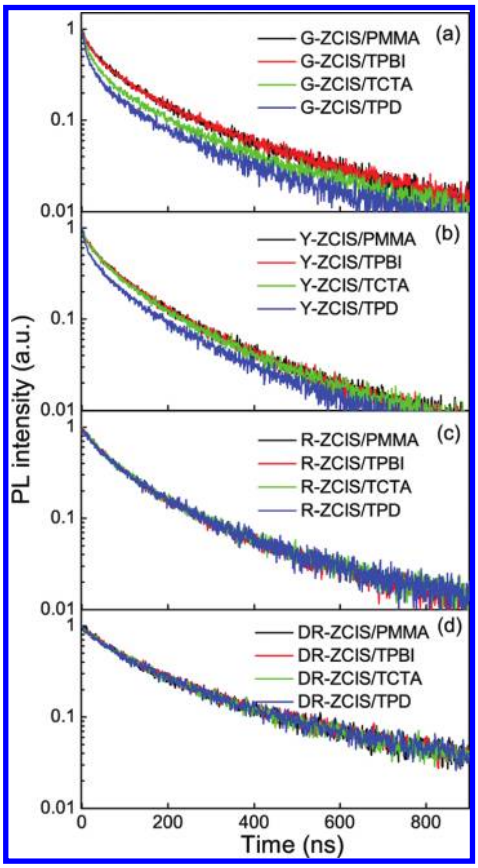

Figure 5. Temporal change of PL intensities of (a) G-, (b) Y-, (c) R-, and (d) DR-ZCIS/ZnS QDs in QD/CTM and PMMA blend films with a QD/organic molecule molar ratio of 1/30. The excitation wavelength is 425 nm.

Y-ZCIS QDs are shortened in TPD matrix due to the charge transfer and show a little change and no change in TCTA and TPBI matrix, compared to that in PMMA matrix, as seen in Figure 5a,b. However, there is no change in the PL decay curves of R- and DR-QDs in TPD (TCTA, TPBI) films, as seen in Figure 5c,d, indicating that the charge separation process does not happen in the blend films.

The valence and conduction energy levels of the ZCIS core and the highest occupied molecular orbital (HOMO) and lowest unoccupied molecular orbital (LUMO) levels of TPBI, TCTA, and TPD are shown in Figure 6. The shortening of the PL lifetimes for ZCIS QDs indicates that the charge separation process occurs in Y- and G-QD/TPD (TCTA) hybrid systems, which is dependent on the energy offset between the valence level of the QDs and the HOMO level of the TPD (TCTA).[32] The energy offset is a driving force for the charge separation process at the QD/CTM interface, giving rise to exciton dissociation in QDs. The valence band levels of the QDs tuned by the particle size and composition are determined from −5.61 eV to −5.77 eV by the cyclic voltammetry measurement, as shown in Figure S6 of the Supporting Information. From the previous reports, the HOMO and LUMO levels of CTMs were determined to be −6.2 and −2.8 eV for TPBI, −5.7 and −2.4 eV for TCTA, and −5.4 and −2.2 eV for TPD, respectively.[1,3,7] The type I band alignment at the interface between TPBI and

dx.doi.org/10.1021/jp3037236 | J. Phys. Chem. C 2012, 116, 11973–11979

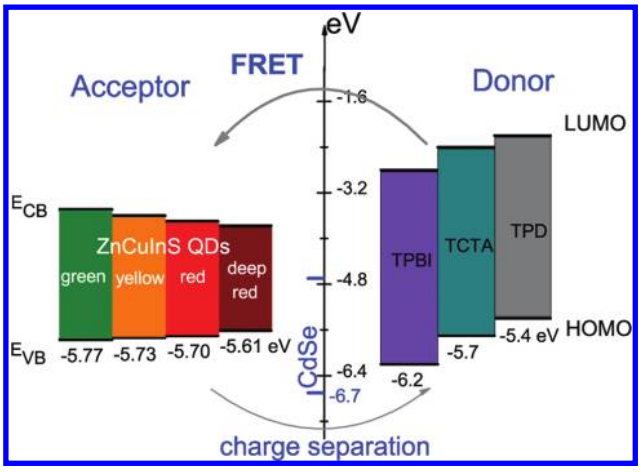

Figure 6. Energy levels of valence and conduction bands for the ZCIS cores, corresponding to ZCIS/ZnS core/shell QDs with green, yellow, red, and deep red emissions, respectively (left), and the HOMO and LUMO levels of TPBI, TCTA, and TPD (right), relative to the vacuum level. The energy levels of valence and conduction bands for the CdSe QDs are also shown in this figure by blue lines.

all the four kind of QDs and the type II alignment at the interface between TPD (TCTA) and QDs with small size and relatively high Zn content can be formed based on the energy difference between the HOMO levels of the CTMs and the valence band levels of ZCIS QDs. The small hole injection barrier (0−0.37 eV) exists between hole transporting materials (TPD and TCTA) and ZCIS alloyed QDs, perhaps improving the performance of the ZCIS QD-LEDs, compared to the large one (~1 eV) between TPD (TCTA) and CdSe QDs (see blue lines in Figure 6).[5,6] Moreover, the small energy offset (driving force) of 0−0.37 eV would also be responsible for a weak charge separation process at the ZCIS QD/TCTA (TPD) interface, identically with the experiment results as shown in Figure 5. This reveals that the heavy metal free ZCIS QDs with the type I or type II band alignment can exhibit efficient energy transfer and/or weak charge separation processes with frequently used CTMs such as TPBI, TCTA, and TPD controlled by varying the particle size and composition of the QDs.

CONCLUSIONS

In summary, we have revealed that the ZCIS alloyed QD/CTM hybrid systems with the type I or type II band alignment exhibit efficient energy transfer process, which can be controlled by varying the QD size and composition. The Förster radius of the ZCIS QD/CTM hybrid films calculated based on the Förster theory is well consistent with the dependence of the energy transfer efficiency on the QDs with various emissions. The size increase and Zn content reduction of ZCIS QDs can enhance the energy transfer efficiency. Therefore, heavy metal-free ZCIS QDs are promising to be used to fabricate high-efficiency and environmentally safe QD-LEDs toward their application in next-generation displays and solid state lighting on the basis of the efficient FRET from organic CTMs to ZCIS QDs.

ASSOCIATED CONTENT

Supporting Information

Preparation of ZCIS core and ZCIS/ZnS core/shell QDs, energy levels of the ZCIS QDs, molar concentration of the ZCIS QDs, TEM images of ZCIS QDs, EDS spectra and the calculated atomic ratio of ZCIS QDs, X-ray diffraction patterns of ZCIS QDs, absorption spectra of TPBI, TCTA, and TPD, normalized PL excitation spectra of G-ZCIS QDs in QD/TPD blend films, and cyclic voltammograms of ZCIS QDs. This material is available free of charge via the Internet at http://pubs.acs.org.

AUTHOR INFORMATION

Corresponding Author

*(J.Z.) Phone: +86-431-86176029. E-mail: zhaojl@ciomp.ac.cn. (Y.M.) Phone: +81-298-534248. E-mail: shoichi@sakura.cc.tsukuba.ac.jp.

Notes

The authors declare no competing financial interest.

ACKNOWLEDGMENTS

This work was supported by the Hundred Talent Program of the Chinese Academy of Sciences, the National Natural Science Foundation of China (No. 10874179, No. 60976049, and No. 51102227), and the Innovative Research Support Program (Pilot Model) of University of Tsukuba, Japan. We thank Professor Junqiao Ding and Professor Zaicheng Sun for their helpful discussions.

REFERENCES

(1) Coe, S.; Woo, W. K.; Bawendi, M. G.; Bulović, V. *Nature* **2002**, *420*, 800−803.
(2) Tessler, N.; Medvedev, V.; Kazes, M.; Kan, S. H.; Banin, U. *Science* **2002**, *295*, 1506−1508.
(3) Zhao, J. L.; Bardecker, J. A.; Munro, A. M.; Liu, M. S.; Niu, Y. H.; Ding, I. K.; Luo, J. D.; Chen, B. Q.; Jen, A. K.-Y.; Ginger, D. S. *Nano Lett.* **2006**, *6*, 463−467.
(4) Li, Y. Q.; Rizzo, A.; Cingolani, R.; Gigli, G. *Adv. Mater.* **2006**, *18*, 2545−2548.
(5) Anikeeva, P. O.; Madigan, C. F.; Halpert, J. E.; Bawendi, M. G.; Bulović, V. *Phys. Rev. B* **2008**, *78*, 085434.
(6) Anikeeva, P. O.; Halpert, J. E.; Bawendi, M. G.; Bulović, V. *Nano Lett.* **2009**, *9*, 2532−2536.
(7) Jing, P. T.; Zheng, J. J.; Zeng, Q. H.; Zhang, Y. L.; Liu, X. M.; Liu, X. Y.; Kong, X. G.; Zhao, J. L. *J. Appl. Phys.* **2009**, *105*, 044313.
(8) Qian, L.; Zheng, Y.; Xue, J. G.; Holloway, P. H. *Nat. Photonics* **2011**, *5*, 543−548.
(9) Greenham, N. C.; Peng, X. G.; Alivisatos, A. P. *Phys. Rev. B* **1996**, *54*, 17628−17637.
(10) Huynh, W. U.; Dittmer, J. J.; Alivisatos, A. P. *Science* **2002**, *295*, 2425−2427.
(11) Xu, T. T.; Qiao, Q. Q. *Energy Environ. Sci.* **2011**, *4*, 2700−2720.
(12) Talapin, D. V.; Lee, J. S.; Kovalenko, M. V.; Shevchenko, E. V. *Chem. Rev.* **2010**, *110*, 389−458.
(13) Castro, S. L.; Bailey, S. G.; Raffaelle, R. P.; Banger, K. K.; Hepp, A. F. *J. Phys. Chem. B* **2004**, *108*, 12429−12435.
(14) Zhong, H. Z.; Zhou, Y.; Ye, M. F.; He, Y. J.; Ye, J. P.; He, C.; Yang, C. H.; Li, Y. F. *Chem. Mater.* **2008**, *20*, 6434−6443.
(15) Xie, R. G.; Rutherford, M.; Peng, X. G. *J. Am. Chem. Soc.* **2009**, *131*, 5691−5697.
(16) Zhong, H. Z.; Lo, S. S.; Mirkovic, T.; Li, Y. C.; Ding, Y. Q.; Li, Y. F.; Scholes, G. D. *ACS Nano* **2010**, *4*, 5253−5262.
(17) Li, L.; Pandey, A.; Werder, D. J.; Khanal, B. P.; Pietryga, J. M.; Klimov, V. I. *J. Am. Chem. Soc.* **2011**, *133*, 1176−1179.
(18) Panthani, M. G.; Akhavan, V.; Goodfellow, B.; Schmidtke, J. P.; Dunn, L.; Dodabalapur, A.; Barbara, P. F.; Korgel, B. A. *J. Am. Chem. Soc.* **2008**, *130*, 16770−16777.
(19) Li, L.; Coates, N.; Moses, D. *J. Am. Chem. Soc.* **2010**, *132*, 22−23.
(20) Zhang, J.; Xie, R. G.; Yang, W. S. *Chem. Mater.* **2011**, *23*, 3357−3361.

(21) Zhang, W. J.; Zhong, X. H. *Inorg. Chem.* **2011**, *50*, 4065−4072.
(22) Feng, J.; Sun, M.; Yang, F.; Yang, X. R. *Chem. Commun.* **2011**, *47*, 6422−6424.
(23) Pan, D. C.; Weng, D.; Wang, X. L.; Xiao, Q. F.; Chen, W.; Xu, C. L.; Yang, Z. Z.; Lu, Y. F. *Chem. Commun.* **2009**, *28*, 4221−4223.
(24) Tan, Z. A.; Zhang, Y.; Xie, C.; Su, H. P.; Liu, J.; Zhang, C. F.; Dellas, N.; Mohney, S. E.; Wang, Y. Q.; Wang, J. K.; Xu, J. *Adv. Mater.* **2011**, *23*, 3553−3558.
(25) Chen, B. K.; Zhong, H. Z.; Zhang, W. Q.; Tan, Z. A.; Li, Y. F.; Yu, C. R.; Zhai, T. Y.; Bando, Y.; Yang, S. Y.; Zou, B. S. *Adv. Funct. Mater.* **2012**, *22*, 2081−2088.
(26) Lakowicz, J. R. *Principles of Fluorescence Spectroscopy*, 3rd ed.; Springer-Verlag: Berlin, Germany, 2006; pp 443−527.
(27) Clapp, A. R.; Medintz, I. L.; Mattoussi, H. *ChemPhysChem* **2006**, *7*, 47−57.
(28) Rogach, A. L.; Klar, T. A.; Lupton, J. M.; Meijerink, A.; Feldmann, J. *J. Mater. Chem.* **2009**, *19*, 1208−1221.
(29) Clapp, A. R.; Medintz, I. L.; Mauro, J. M.; Fisher, B. R.; Bawendi, M. G.; Mattoussi, H. *J. Am. Chem. Soc.* **2004**, *126*, 301−310.
(30) Sadhu, S.; Patra, A. *Appl. Phys. Lett.* **2008**, *93*, 183104.
(31) Lunz, M.; Bradley, A. L.; Gerard, V. A.; Byrne, S. J.; Gun'ko, Y. K. *Phys. Rev. B* **2011**, *83*, 115423.
(32) Lutich, A. A.; Jiang, G. X.; Susha, A. S.; Rogach, A. L.; Stefani, F. D.; Feldmann, J. *Nano Lett.* **2009**, *9*, 2636−2640.
(33) Jing, P. T.; Yuan, X.; Ji, W. Y.; Ikezawa, M.; Wang, Y. A.; Liu, X. Y.; Zhang, L. G.; Zhao, J. L.; Masumoto, Y. *J. Phys. Chem. C* **2010**, *114*, 19256−19262.
(34) Jing, P. T.; Yuan, X.; Ji, W. Y.; Ikezawa, M.; Liu, X. Y.; Zhang, L. G.; Zhao, J. L.; Masumoto, Y. *Appl. Phys. Lett.* **2011**, *99*, 093106.
(35) Moreels, I.; Lambert, K.; Muynck, D. D.; Vanhaecke, F.; Poelman, D.; Martins, J. C.; Allan, G.; Hens, Z. *Chem. Mater.* **2007**, *19*, 6101−6106.
(36) Yu, W. W.; Qu, L. H.; Guo, W. Z.; Peng, X. G. *Chem. Mater.* **2003**, *15*, 2854−2860.
(37) Anni, M.; Manna, L.; Cingolani, R.; Valerini, D.; Cretí, A.; Lomascolo, M. *Appl. Phys. Lett.* **2004**, *85*, 4169. **2006**, *88*, 259901.
(38) Anikeeva, P. O.; Madigan, C. F.; Coe-Sullivan, S. A.; Steckel, J. S.; Bawendi, M. G.; Bulović, V. *Chem. Phys. Lett.* **2006**, *424*, 120−125.
(39) Kaufmann, S.; Stöferle, T.; Moll, N.; Mahrt, R. F.; Scherf, U.; Tsami, A.; Talapin, D. V.; Murray, C. B. *Appl. Phys. Lett.* **2007**, *90*, 071108.
(40) Chin, P. K.; Hikmet, R. M.; Janssen, R. J. *J. Appl. Phys.* **2008**, *104*, 013108.